September 2008
SLAC-PUB-13406

# High Harmonic Generation from Multiple Orbitals in $N_2$

Brian K. McFarland, Joseph P. Farrell, Philip H. Bucksbaum, Markus Gühr*

PULSE Institute, Stanford Linear Accelerator Center, Menlo Park, CA 94025, USA
and Physics Department, Stanford University, Stanford, CA 94305, USA

*To whom correspondence should be addressed; E-mail: mguehr@stanford.edu

**Molecular electronic states energetically below the highest occupied molecular orbital (HOMO) should contribute to laser-driven high harmonic generation (HHG), but this behavior has not been observed previously. Our measurements of the HHG spectrum of $N_2$ molecules aligned perpendicular to the laser polarization show a maximum at the rotational half revival. This feature indicates the influence of electrons occupying the orbital just below the $N_2$ HOMO, referred to as the HOMO–1. Such observations of lower-lying orbitals are essential to understanding the sub-femtosecond/sub-angstrom electronic motion in laser excited molecules.**

Tomographic imaging of molecules using high harmonic generation (HHG) has attracted wide interest [1]. The method can be easily described in the framework of a strong-field three-step model [2, 3]. In this model, a portion of the electron wave function corresponding to the highest occupied molecular orbital (HOMO) tunnels into the continuum and is accelerated in a strong oscillating optical field. This continuum part of the wave function is treated as a free electron wave packet, which interferes coherently with the bound part of the HOMO when it returns to the molecule. Recombination dipole radiation is emitted on every half-cycle of the driving field and the coherent superposition of this radiation over multiple cycles forms a discrete spectrum of odd-order high harmonics. The spectrum contains information about the HOMO structure. Tomographic reconstruction achieves sub-angstrom spatial resolution de-



Published in the Science
Work supported in part by US Department of Energy contract DE-AC02-76SF00515

termined by the shortest de Broglie wavelength of the recombining electrons. The harmonics also carry sub-femtosecond timing information due to the sub-cycle electron recombination. This high temporal and spatial resolution can enable ultrafast movies of molecular orbital dynamics; however to date, only the stationary HOMO has been imaged. Electron dynamics result from the coherent superposition of multiple electronic stationary states. Observing sub-femtosecond electron dynamics therefore requires the participation of multiple orbitals in HHG.

Here we report simultaneous HHG from two molecular electronic orbitals, the HOMO and the next lower bound HOMO–1 in $N_2$. The HOMO–1 participation emerges through enhancements in the HHG signal at characteristic alignment angles of the molecular axis to the polarization of the harmonic generating pulse. The angular alignment is accomplished by impulsive rotational excitation of a cold (40K) and dense $N_2$ jet by a nonresonant femtosecond laser pulse [4]. In the vicinity of a rotational revival, the molecules undergo a rapid change in alignment with respect to the polarization of a second laser which produces HHG. Although in our experiment low order harmonics (15-25) show a weakening of the harmonic signal if the molecular axis is perpendicular to the harmonic generation polarization, at higher harmonic orders a peak appears that is highly pronounced in this configuration. We attribute the minimum amplitude in the low harmonics to HHG derived predominantly from the HOMO; the peak at higher harmonics is characteristic of HHG from the HOMO–1. The prominent peak at higher harmonics shows three important features of the HOMO–1 that are predicted by semiclassical simulations and simple ionization arguments: the cutoff extends to shorter wavelengths compared to an isotropic ensemble; it is strongest when the molecular axes are near $90^o$ to the harmonic generation polarization; and it presents itself most clearly near the cutoff.

Past studies of HHG from aligned $N_2$ concentrated on the plateau region for orbital reconstruction [1] and not on the cutoff region where the HOMO–1 signal is most pronounced. We observe that the HOMO–1 signal is very sensitive to the molecular alignment and we tune our alignment parameters to optimize the signal.

The preferential field ionization of a more deeply bound state over a less deeply bound state is possible because of the different geometries of the corresponding wave functions in the molecular frame. This scenario is analogous to the field ionization of Stark states in atoms, where $m_l = 0$ states ionize more easily than $m_l > 0$ states because the $m_l = 0$ states overlap the saddle-point in the potential [5]. Field ionization is most sensitive to the outer parts of the electron wave function near this saddle point [6]. Figure 1A illustrates this point with cuts through isoprobability density surfaces of the HOMO (solid line) and HOMO–1 (dashed line) of $N_2$. The color indicates the relative sign of the wave function amplitude. The orbitals are obtained by ab-initio calculations using an STO-3G basis set in the Gaussian software package [7]. The $N_2$ HOMO and HOMO–1 exhibit $\sigma_g$ and $\pi_u$ symmetries, respectively. The cuts through the HOMO and HOMO–1 orbitals show that the HOMO extends farther than the HOMO–1 along the direction parallel to the internuclear axis. Therefore the HOMO will preferentially ionize when the electric field is parallel to the internuclear axis. The situation is reversed in the direction perpendicular to the internuclear axis, where the HOMO–1 protrudes farther than the HOMO. This property is further demonstrated in Fig. 1B which gives 1D cuts through the orbitals along the black dashed line in Fig. 1A. We conclude that the lower bound HOMO–1 ionizes more easily than the HOMO when the laser field is polarized $90^o$ with respect to the internuclear axis. This conclusion is supported by a strong field ionization calculation for the HOMO and HOMO–1 orbitals [8].

Following strong-field ionization of a particular orbital, the acceleration of the electron in the laser field results in an energy dispersed (chirped) electron wave packet. The recombining electron wave packet is therefore a de Broglie wave, $\Phi_{free}$, whose instantaneous wavelength $\lambda_{dB}$ changes as a function of recombination time. The returning electron wave forms a superposition with the $N_2$ orbital, inducing a time dependent dipole moment described by $\langle HOMO|ez|\Phi_{free}\rangle$ or $\langle HOMO\text{–}1|ez|\Phi_{free}\rangle$ for the respective orbital, as it moves across the $N_2$ molecule. Figure 1C sketches the recombination step for molecules standing parallel to the harmonic generation polarization. Recombination to the HOMO gives rise to a large dipole since the expectation value of z can vary all along the long axis of the HOMO [1].

The HOMO–1, however, will not produce any signal because the nodal structure reduces recombination probability [9] and, in addition, the opposite parity of the two HOMO–1 lobes produces two dipoles that cancel because of a $\pi$ phase shift.

For recombination with the generation laser polarization perpendicular to the internuclear axis (Fig. 1D), the electron distribution of the HOMO is considerably more confined and yields a diminished dipole moment compared with the parallel case. The HOMO–1 on the other hand is less confined than the HOMO and will give rise to a correspondingly stronger time dependent dipole moment. We neglect dipoles perpendicular to the harmonic generation polarization because they are not phase matched for alignment ensembles with mirror symmetry around the plane formed by the harmonic generation polarization and propagation vector of the laser pulse [10].

In order to optimize the HOMO–1 signal, the molecular axes need to be aligned perpendicular to the generation field. We can achieve this through impulsive alignment in two different ways: The alignment and generation polarizations can be set parallel, which leads to an anti-aligned ensemble just past the half revival (4.4 ps) where the molecules are perpendicular to the laser polarization. Alternatively, the laser polarizations can be perpendicular in which case a prolate (see Fig. 2C) ensemble with the desired alignment occurs at the half revival (4.1 ps). We found that an alignment scheme with perpendicular polarizations enhances the contrast of the HOMO–1 with respect to the HOMO.

The HOMO–1 has a characteristic spectral signature. Due to the larger ionization potential (IP) of the HOMO–1, we expect the HOMO–1 to have a higher cutoff than the HOMO. The HHG cutoff is given by 3.17$U_p$+IP, where $U_p$ is the ponderomotive energy [2].

Figure 2A shows a diagram of the experiment. We split the output of a 1kHz, 30 fs Ti:Sapphire laser system into two time-delayed pulses using a wavefront beam splitter. The first pulse (alignment pulse, 90 fs for optimal alignment, intensity $I_{align}$ = 2.5$\times 10^{13}$ W/cm$^2$) aligns the molecules, and the second (generation pulse, 30 fs, intensity $I_G$ = 1.7 to 2.3$\times 10^{14}$ W/cm$^2$) generates harmonics from the aligned molecules. The pulses are focused with a spherical mirror (R = 800 mm) into a supersonically cooled

gas jet of $N_2$ molecules in vacuum. The jet is positioned about 2 mm beyond the focus for optimal phase matching [11]. The long alignment pulse excites a rotational wave packet in the molecules, leading to periodic field-free alignment [4]. We examine the high harmonics generated near the half revival around 4.1 ps where constructive interference of the rotational coherence for $N_2$ leads to a strong modulation of the alignment parameter $\langle \cos^4 \theta \rangle$ [12]. Here $\theta$ is the angle between the alignment laser polarization and the internuclear axis. The lower part of Fig. 2B shows the calculated value of $\langle \cos^4 \theta \rangle$ for a rotational temperature of T = 40 K, and an alignment laser intensity of $I_{align}$ = 2.5×$10^{13}$ W/cm$^2$. The harmonics between 20 and 70 eV pass through an Al filter (thickness 100 nm) into an imaging spectrometer where the harmonics that are phase matched on axis ("short" trajectories) are selected by an aperture [13].

Figure 2B shows a false color plot of harmonic spectra collected for different delays between the perpendicularly polarized alignment pulse and the harmonic generation pulse. The odd harmonics of the fundamental radiation from the 15th to the 39th (cutoff) harmonic are modulated along the time axis by the rotational revivals. The character of this modulation is similar for the lower harmonics but changes for harmonics in the cutoff region. Specifically, the signal suppression in the plateau harmonics near 0.25 ps and 4.1 ps becomes an enhancement for cutoff harmonics.

We integrate over the center portion of each harmonic peak and normalize to the baseline alignment signal. The resulting integrated harmonic signals are plotted from 3.5 to 4.7 ps time delays in Fig. 3A for three values of the generation intensity $I_G$. Concentrating on $I_G$ = 2.3×$10^{14}$ W/cm$^2$, revival traces are plotted for harmonic 15, and 25 to 39, with the cutoff at harmonic 39. Harmonics 15 to 23 have the same shape, and we plot harmonic 15 as a representative of these curves. Starting at harmonic 25, the minimum at 4.1 ps begins to flatten and harmonics 31 and greater show a peak superimposed on the minimum. At harmonic 39, the temporal structure is completely inverted compared with the trend seen for harmonic 15.

A comparison with the $\langle \cos^4 \theta \rangle$ characteristics in Fig. 2B shows that the harmonic signal is modulated by the molecular revival structure induced by the alignment pulse. The 15th to 25th harmonics

have a minimum at 4.1 ps when a prolate alignment distribution appears in the direction perpendicular to the generation polarization. A maximum occurs at 4.4 ps when an oblate distribution appears in the plane orthogonal to the alignment polarization (see Fig. 2C). The alignment distribution and the ionization and recombination characteristics of the $N_2$ HOMO explain these revival signals. The minimum in the revival signal at 4.1 ps occurs when alignment perpendicular to the generation laser polarization is largest. As explained above, we expect low ionization and a small recombination dipole for the HOMO under these conditions. At 4.4 ps alignment parallel to the HHG laser polarization is largest, resulting in more ionization, a larger recombination dipole and thus a maximum in the HHG from the HOMO. These observations connect the revival signal in harmonics 15 to 25 to HHG from the HOMO.

A different phenomenon is revealed for harmonics 25 and greater. As described above, a peak grows out of the minimum at 4.1 ps leading to the inverted structure at harmonic 39. This peak is indicative of HHG from the HOMO–1. We expect ionization and recombination to be stronger for the HOMO–1 compared with the HOMO when the molecular ensemble is oriented $90^o$ to the generation laser polarization. Furthermore, the HOMO–1 signal should dominate at harmonic 39 because of the extended cutoff. We show below that the evolution of this feature with harmonic number is also consistent with high harmonics from the HOMO–1. The revival structures in harmonics 25 to 35 show attributes of both HOMO and HOMO–1 harmonic generation where the HOMO contribution is strongest for the low harmonics and the contribution from the HOMO–1 becomes prominent in the high harmonics.

The dependence of the HOMO–1 peak on $I_G$ was studied by introducing pellicle beam splitters without changing the alignment intensity or any other parameter. The temporal modulation of each harmonic changes with $I_G$. For example, the 33rd harmonic for the highest $I_G$ shows a valley at 4.1 ps and a peak at 4.4 ps attributed to the HOMO, superimposed on the peak at 4.1 ps attributed to the HOMO–1. At $I_G$ = 1.9x$10^{14}$ W/cm$^2$ the same harmonic only shows the HOMO–1 peak; the HOMO features are absent.

Our results bare some similarities to previous reports of inversions of the alignment-dependent signal

in $CO_2$, which were attributed either to interference effects [14] or to ionization depletion [15, 16]. The aspects of the present work that allow us to eliminate these explanations cleanly are the perpendicular geometry and the striking dependence of our spectra on the generating pulse intensity. The interference model proposed in the previous work by [14] explains their observations for $CO_2$ consistently and does not predict a change of the revival structure with $I_G$. In contrast, we observe that the revival structure of $N_2$ depends on $I_G$, strongly suggesting the involvement of different orbitals that we propose. Furthermore, ionization depletion effects that have been observed and analyzed in [15, 16] lead to specific predictions for the harmonic intensity dependence on $I_G$. In our geometry of a prolate ensemble aligned perpendicular to the generation polarization, the ionization depletion model predicts an increasing harmonic signal for increasing $I_G$. This is opposite to the trend we observe at 4.1 ps in Fig. 3A (see for example harmonic 29). Therefore, we rule out either of these alternative explanations for our data.

These simple arguments for multiple orbital contributions are supported by semiclassical simulations of the recombination process in HHG. Details of our simulation procedures can be found in [17]. The phase of a free electron wave $\Phi_{free}$ is calculated by integrating the Lagrangian of an electron in the electric field, neglecting the shape of the molecular potential (strong field approximation). We calculate the dipole $\langle HOMO|ez|\Phi_{free}\rangle$ or $\langle HOMO\text{–}1|ez|\Phi_{free}\rangle$ for multiple angles $\alpha$ between the molecular axis and the propagation vector of the recombining wave (z axis) and superimpose them according to the calculated prolate molecular distribution at 4.1 ps [18]. The dipoles are Fourier transformed and multiplied by $\omega^4$ [19]. Since we only take one ionization-recombination event into account we obtain the envelope of the harmonics in Fig. 3B.

We estimate ionization and electron dispersion to have a small effect on the relative HHG amplitudes of the HOMO and HOMO–1 via the following argument. The dependence of the $N_2$ ionization on the angle between the ionizing laser polarization and the alignment distribution has been studied [20]. A comparison of this experimental result with the angular ionization dependence of the HOMO calculated with the MO-ADK method [6, 20] allows us to estimate that the HOMO–1 has between 2 to 3.5 times

the ionization rate of the HOMO. In addition, the dispersion of the free electron wave in the direction perpendicular to its propagation is greater for the HOMO–1 compared to the HOMO, since the HOMO–1 is more compact (contains higher momentum components). The trends of ionization and dispersion are opposite and we do not expect them to change the ratio of the HOMO to HOMO–1 HHG signal considerably.

The HHG spectrum for the HOMO (black) has a clearly visible plateau and a cutoff at 60 eV, matching the prediction of the cutoff law at $I_G = 2.3\times10^{14}$ W/cm$^2$. In the HOMO–1 spectrum (red), the plateau region is reduced. The HOMO–1 spectral amplitude is small for low photon energies, but increases in the cutoff region, in agreement with the experiment. The HHG cutoff for the HOMO–1 extends beyond that of the HOMO by more than can be explained by the 1.3 eV difference in IP. It is now well-established that the shape of a molecular wave function has a strong effect on the HHG spectrum [14, 21, 22, 23]. This is the primary reason for the relative enhancement of the HOMO–1 component of the HHG signal in our experiment. The model in [21] applied to the antisymmetric HOMO–1 predicts an HHG enhancement for the condition $\Delta = \lambda_{dB}/2$, where $\Delta$ is the separation between the two antinodes in the wave function along the direction of the returning electron k-vector. For a prolate molecular distribution the prominent direction is $\alpha = 90^o$ which results in $\Delta$ = 1.74 $a_0$. The electron recombines releasing a photon whose energy is equal to the sum of the electron kinetic energy and the ionization potential, and so this $\lambda_{dB}$ of 3.48 $a_0$ leads to a maximum at 60 eV in the emitted spectrum. For molecules with smaller $\alpha$, which are also present in the prolate distribution, $\Delta$ becomes larger. This results in a shift of the constructive interference to larger $\lambda_{dB}$ and smaller photon energies. Therefore, we expect a strong contribution from the HOMO–1 in the energy range around and below 60 eV as seen in Fig. 3B. The cutoff for our intensities lies in this energy range and we observe an agreement between the calculation and the data in Fig. 3. The full width at half maximum of the HOMO–1 spectrum in the constructive interference region is 20 eV for the highest $I_G$ and about 10 eV for the lowest $I_G$. This trend agrees with the experiment: the HOMO–1 feature is prominent from harmonic 25 to 39 corresponding to a width of 22 eV for the highest

$I_G$; for the lowest $I_G$ the peak appears from harmonic 25 to 31 corresponding to a width of 9 eV.

## References


[1] J. Itatani, J. Levesque, D. Zeidler, H. Niikura, H. Pepin, J. C. Kieffer, P. B. Corkum, and D. M. Villeneuve, *Nature* **432**, 867 (2004).

[2] P. B. Corkum, *Phys. Rev. Lett.* **71**, 1994 (1993).

[3] K. C. Kulander, K. J. Schafer, and J. L. Krause, *Laser Phys.* **3**, 359 (1993).

[4] H. Stapelfeldt and T. Seideman, *Rev. Mod. Phys.* **75**, 543 (2003).

[5] Th. F. Gallagher, *Rydberg Atoms* (Cambridge Univ. Press, Cambridge, 1994).

[6] X. M. Tong, Z. X. Zhao, and C. D. Lin, *Phys. Rev. A* **66**, 33402 (2002).

[7] M. J. Frisch et al., Gaussian 03, Revision C.02. Gaussian, Inc., Wallingford, CT, 2004.

[8] V. I. Usachenko and S. I. Chu, *Phys. Rev. A* **71**, 063410 (2005).

[9] M. Spanner, O. Smirnova, P. B. Corkum, M. Y. Ivanov, *J. Phys. B***37**, L243 (2004).

[10] J. Levesque, Y. Mairesse, N. Dudovich, H. Pepin, J. C. Kieffer, P. B. Corkum, and D. M. Villeneuve, *Phys. Rev. Lett.* **99**, 243001 (2007).

[11] P. Balcou, P. Salières, A. LHuillier, and M. Lewenstein, *Phys. Rev. A* **55**, 3204 (1997).

[12] S. Ramakrishna and T. Seideman, *Phys. Rev. Lett.* **99**, 113901 (2007).

[13] P. Salières, A. L'Huillier, and M. Lewenstein, *Phys. Rev. Lett.* **74**, 3776 (1995).

[14] X. Zhou, R. Lock, W. Li, N. Wagner, M. M. Murnane, and H. C. Kapteyn, *Phys. Rev. Lett.* **100**, 073902 (2008).

[15] A. T. Lee, X. M. Zhao, and C. D. Lin, *Phys. Rev. A* **73**, 041402 (2006).

[16] P. Liu, P. Yu, Z. Zeng, H. Xiong, X. Ge, R. Li, and Z. Xu, *Phys. Rev. A* **78**, 015802 (2008).

[17] M. Gühr, B. K. McFarland, J. P. Farrell, and P. H. Bucksbaum, *J. Phys. B* **40**, 3745 (2007).

[18] J. Ortigoso, M. Rodriguez, M. Gupta, and B. Friedrich, *J. Chem. Phys.* **110**, 3870 (1999).

[19] J. Levesque, D. Zeidler, J. P. Marangos, P. B. Corkum, and D. M. Villeneuve, *Phys. Rev. Lett.* **98**, 183903 (2007).

[20] D. Pavicic, K. F. Lee, D. M. Rayner, P. B. Corkum, and D. M. Villeneuve, *Phys. Rev. Lett.* **98**, 243001 (2007).

[21] M. Lein, N. Hay, R. Velotta, J. P. Marangos, and P. L. Knight, *Phys. Rev. A* **66**, 023805 (2002).

[22] T. Kanai, S. Minemoto, and H. Sakai, *Nature* **435**, 470 (2005).

[23] C. Vozzi, F. Calegari, E. Benedetti, J. P. Caumes, G. Sansone, S. Stagira, M. Nisoli, R. Torres, E. Heesel, N. Kajumba, J. P. Marangos, C. Altucci, and R. Velotta, *Phys. Rev. Lett.* **95**, 153902 (2005).

24. We thank H. Merdji and O. Smirnova for insightful discussions. This work is supported by the U.S. Department of Energy Division of Basic Energy Sciences through the Stanford Linear Accelerator Center. MG thanks the Humboldt Foundation for a fellowship.

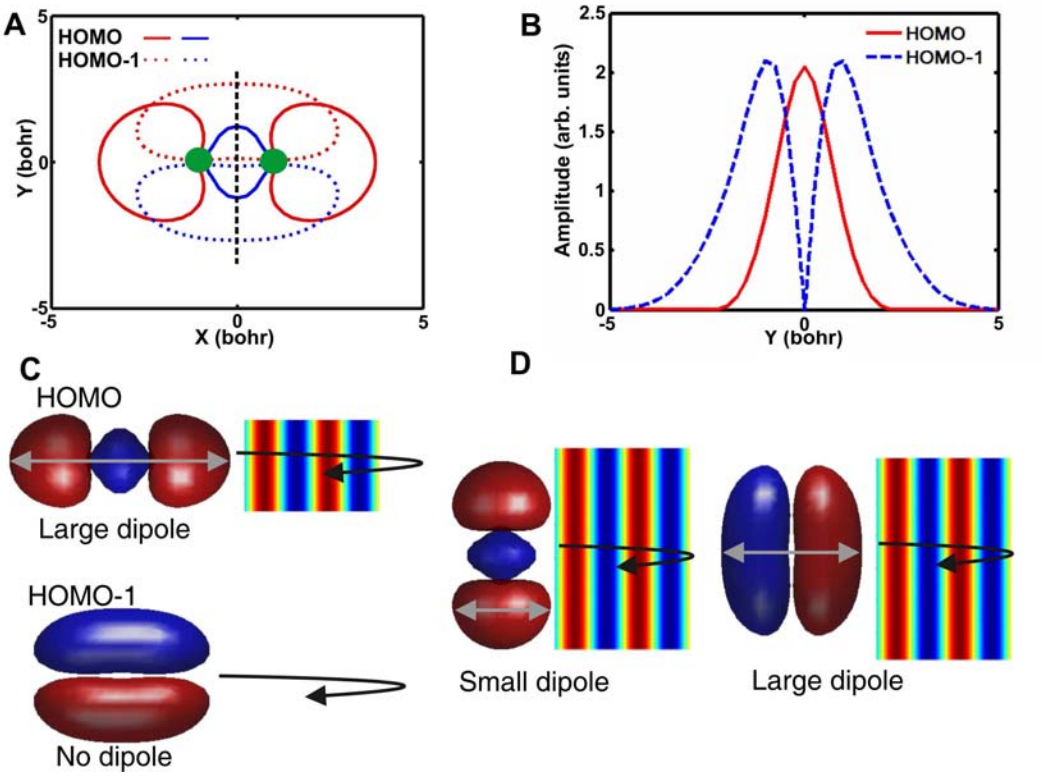


Figure 1: A) Isoamplitude lines of the $N_2$ HOMO (solid lines) and HOMO–1 (dashed lines). The color indicates the sign of the wave function. The green disks indicate the position of the nuclei. B) Absolute amplitude of the HOMO (solid red line) and the HOMO–1 (dashed blue line) along a direction perpendicular to the internuclear axis, indicated by the black dashed line in A. C) Sketch of the recombining free electron wave for the electric field creating the high harmonics polarized along the internuclear axis. A strong dipole is induced in the HOMO, whereas no dipole is induced in the HOMO–1 (see text). D) Same sketch as in C for harmonic generating field polarized perpendicular to the internuclear axis. Compared with C, the dipole for the HOMO is weakened, whereas the HOMO–1 dipole is strengthened.

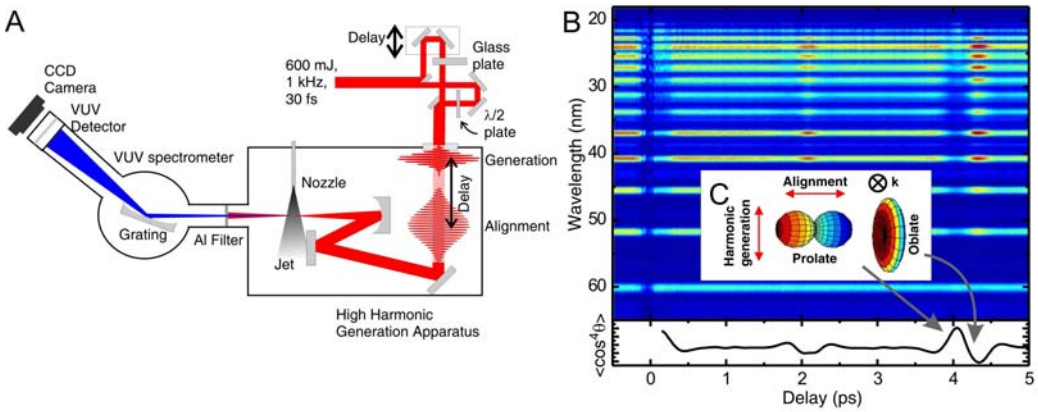


Figure 2: A) Experimental setup. The 600 $\mu$J, 30 fs pulse is split into alignment and generating pulses with variable relative delay. The alignment pulse is chirped by a glass plate to 90 fs. The relative polarization can be set to $90^o$ by a $\lambda/2$ plate. The alignment pulse excites a rotational wave packet in the molecules in a supersonic gas jet and the delayed generation pulse produces high harmonics from the molecules. The light is dispersed by a flat-field toroidal grating (300 lines/mm) and collected by a MCP-phosphor screen detector viewed by a CCD camera. B) Upper panel: Harmonic spectrum as a function of alignment-generation delay in a false color plot (blue: low signal, red: large signal). Lower panel: the calculated expectation value $\langle \cos^4 \theta \rangle$, where $\theta$ is the angle between the alignment laser polarization and the internuclear axis. C) Inset showing the angular distributions at the half-rotational revival, having axial symmetry around the alignment polarization. At 4.1 ps the molecular axis distribution has a prolate shape around the alignment polarization; at 4.4 ps after the alignment pulse it has an oblate shape. The polarizations of the alignment and generation pulses are indicated by the arrows. The k-vectors of the pulses point into the page.

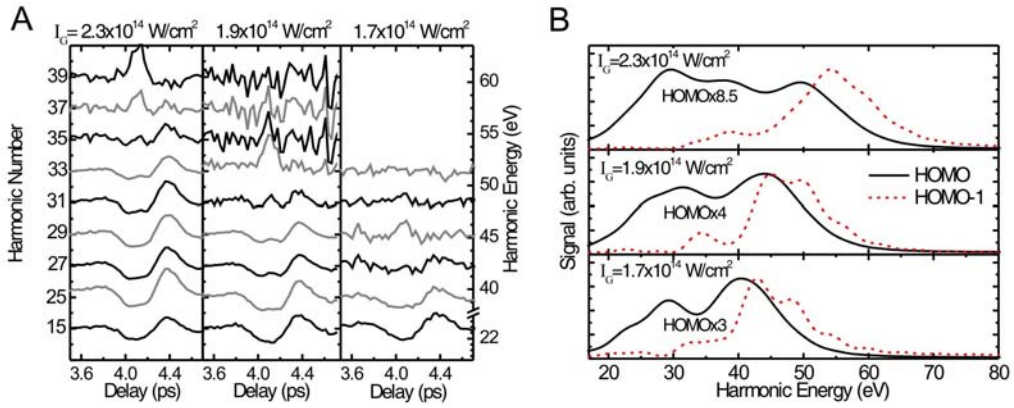


Figure 3: A) Experimental harmonic signals for three different generation intensities $I_G$. The signals are normalized to the harmonic signal of an isotropic ensemble. Therefore, the weak signals in the cutoff are magnified. The cutoffs are located at harmonic 39, 35 and 31 for the three intensities shown. For harmonic 15, a minimum at 4.1 ps is followed by a maximum at 4.4 ps. At higher harmonics, a peak grows out of the minimum at 4.1 ps due to ionization from and recombination to the HOMO–1 (see text). B) Simulations of the experimental harmonic spectral envelope for the three different generation intensities of A, considering only the recombination step. We simulated the prolate molecular distribution used in the experiment. The HOMO–1 spectrum (red dashed) has a larger amplitude than that of the HOMO (black) in the cutoff region. The HOMO HHG signal is scaled by the factors shown in the figure.